ACS Photonics

Article

pubs.acs.org/journal/apchd5

Suppressed Percolation in Nearly Closed Gold Films

Stefano De Zuani,[†] Marcus Rommel,[‡,§] Bruno Gompf,[*,†] Audrey Berrier,[†] Jürgen Weis,[‡] and Martin Dressel[†]

[†]1. Physikalisches Institut and Research Center SCoPE, Universität Stuttgart, Pfaffenwaldring 57, 70569 Stuttgart, Germany

[‡]Max Planck Institute for Solid State Research, Heisenbergstrasse 1, 70569 Stuttgart, Germany

Supporting Information

ABSTRACT: Metal−dielectric composites exhibit remarkable properties at the percolation threshold. A small variation of the filling factor can lead to a huge variation in the dc conductivity from an insulator-like to a metal-like behavior while the real part of the permittivity diverges. This behavior can, in principle, be described by percolation theories at low frequencies and by effective medium approximations at higher frequencies. These theories assume a random distribution of the metallic inclusions inside the insulating matrix. But what happens in ordered structures when the percolation is deliberately suppressed? Even though a simple, nanometer-wide scratch can deteriorate the dc conductivity of a thin metal film, can it influence the mirror-like reflectivity? To address this question, we perform a systematic ellipsometric investigation on nearly closed Au films interrupted only by a two-dimensional periodic mesh of 20 nm wide lines. These nanostructured films have metal filling factors close to unity, but exhibit no dc conductivity. In the infrared, they show an antireflective behavior that can be tuned through the mesh periodicity. Surprisingly, the optical response of these structures can be modeled quite well by simple effective medium approximations. Increasing the size of the squares leads to a tunable, diverging, real part of the permittivity: a maximum of the real part of the permittivity of 1420 is found for the largest investigated squares in this study.

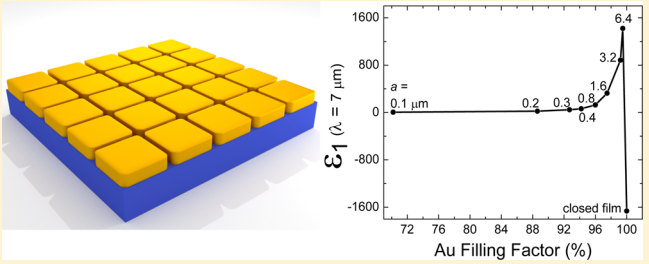

KEYWORDS: *percolation, spectroscopic ellipsometry, antireflective properties, effective medium theory*

In the last two centuries, many theories have been developed and improved to achieve a better description and understanding of the properties of heterogeneous composites made of metal particles embedded in a dielectric matrix.[1] Even though computational electromagnetics enables us to better examine the influence of the randomness and connectedness of metallo-dielectric composites, the disadvantage of this approach is that solving Maxwell's equations for complex, three-dimensional (3D) structures for a variety of angles of incidence and a broad frequency range is still very time-consuming. In particular, the critical evaluation of the validity limit of the modeling with effective optical parameters is still very challenging in the case of complex, heterogeneous samples. For these reasons, the Bruggeman effective medium approximation (BEMA)[2] and the percolation theory[3] are often used because they provide analytical predictions of the effective optical response of random composites by means of very few critical parameters. However, the BEMA is expected to fail for instance around the percolation threshold, i.e., at the critical filling factor f_c where the insulator-to-metal transition occurs.[3] There, the assumption of a homogeneous background field breaks down and hot spots appear, dominating the linear and nonlinear optical properties.[4] For example, for a random distribution of spherical inclusions, the BEMA predicts f_c at 0.33, whereas from percolation theory f_c is expected to be at the Scher−Zallen critical value of about 0.15.[5] Independently of the theoretical approach, the main aim of most of the research in this field is to understand "real" samples, where "real" means samples consisting of inclusions with a broad variety of sizes and shapes randomly distributed in a matrix. The most prominent examples are ultrathin metal films prepared under well-defined evaporation conditions. In principle, they can be described by effective optical parameters. Counterintuitively, below the percolation threshold they can act as antireflecting coatings, and at the percolation threshold, the real part of the permittivity diverges, reaching extremely high positive values.[6,7] While random metal−dielectric composites undergo an insulator-to-metal transition at f_c, what happens when the percolation transition is intentionally suppressed, i.e., when f_c is intentionally pushed toward 1? Can the BEMA theory be applied even in the extreme case of a filling factor close to 1? Nowadays, nanolithographic techniques allow the preparation of artificial nanostructures with a well-defined geometry on a nanometer scale. Nevertheless up to now, little has been done in the field of controlled percolation. In principle, one can think of two extreme cases: the first case corresponds to a very thin and long metallic wire connecting two electrodes, where the sample exhibits a dc conductivity while the filling factor is nearly zero, hence without metallic reflectivity in the near-

Received: March 18, 2016
Published: May 10, 2016

DOI: 10.1021/acsphotonics.6b00198
ACS Photonics 2016, 3, 1109−1115

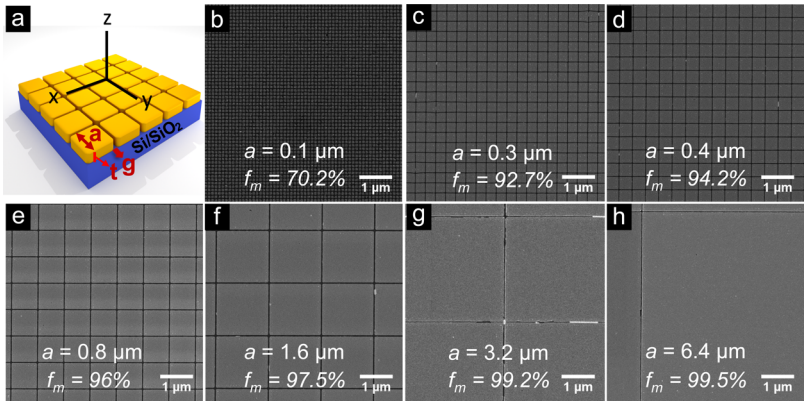

Figure 1. (a) Schematic drawing representing gold square array with square size a, thickness t, and gap width g on a Si/SiO_2 substrate. (b–h) SEM images (6×6 μm^2) of seven different square patterns with thickness t = 20 nm and lateral sizes a ranging from (b) 0.1 μm to (h) 6.4 μm as indicated. The gap g is roughly 20 nm for all samples. The gold filling factor f_m extracted from the analysis of the SEM images increases with increasing square size a from (b) 70% to (h) 99.5%.

infrared range. This situation can be nicely approximated, for example, by self-similar curves, e.g., Hilbert curves.[8] The other extreme case is a closed metallic layer with a nanometer-wide cut preventing dc conductivity although the filling factor is nearly 1. This is the topic of the present report.

Here we present a systematic study on thin Au films interrupted only by a two-dimensional periodic mesh of 20 nm wide gaps forming disconnected squares of size a and presenting very large gold filling factors. Eleven different samples were investigated with reflection measurements and spectroscopic ellipsometry in the wavelength range between 400 and 7000 nm. The samples consist of 20 nm thick nearly closed gold films, formed by disconnected gold squares fabricated on SiO_2/Si substrates over large areas, with a nominal square size a varying from 0.1 to 6.4 μm, separated by gaps of width g of roughly 20 nm, which is kept constant for all samples (Figure 1). We show that, despite the fact that their entire surface is almost completely formed by a 20 nm thick gold layer, which is highly reflective in the infrared frequency range, a strongly decreased reflectance is observed in a broad wavelength range from 1 up to 7 μm. We also demonstrate that the minimum of the reflectance can be tuned by increasing a. Moreover we report how, even for gold filling factors above 90%, the measured reflectance is significantly affected by the presence of a few gaps, and it strongly differs from that of a completely closed 20 nm thick gold film. Finally we show that, despite the fact that our structures are two-dimensional inverted gratings with a period comparable to the wavelength of the incident light, surprisingly it is still possible to model the optical response of these samples by a simple isotropic BEMA model. By intentionally suppressing the percolation, extremely high values of the real part of the dielectric function can be reached through the precise control of the metal filling factor f, obtained by varying the periodicity of the gaps.

SAMPLE DESCRIPTION

The square patterns were fabricated by electron-beam lithography on a silicon wafer covered by a thermally grown, 300 nm thick SiO_2 layer.[9] The fabrication process allows us to precisely control the width of the gaps down to 20 nm and to obtain large patterned areas (1.5×1.5 mm or larger). The large sample sizes are necessary in order to perform angular-dependent reflectance and spectroscopic ellipsometry measurements with a well-defined k-vector up to large angles of incidence. We fabricated 11 samples increasing the gold filling factor f_m by changing the nominal size of the squares a from 0.1 to 6.4 μm and keeping the gap g constant at 20 nm. In this way the gold filling factor f_m extracted from the analysis of the scanning electron microscope (SEM) images increases from 70.2% for the squares of size $a \approx 0.1$ μm up to 99.5% for the sample with size a = 6.4 μm. Figure 1a illustrates the three-dimensional design of the samples. The SEM images of seven different gold square patterns are exhibited in Figure 1b–h on a uniform scale.

EXPERIMENTAL RESULTS

Three different sets of measurements were performed on the samples: (1) spectroscopic ellipsometric measurements in the spectral range between 400 and 2200 nm at angles of incidence varying between 40° and 60° in steps of 5° with the plane of incidence parallel to the meshes; (2) oblique incidence reflection measurements with p-polarized light in the range 400 to 2200 nm and angles of incidence between 30° and 70° in steps of 2°, both measurements 1 and 2 being performed with a Woollam variable-angle spectroscopic ellipsometer (WVASE); (3) reflectance measurements at normal incidence using unpolarized light in the spectral range between 600 and 7000 nm performed with a Bruker IFS 66/s Fourier-transform infrared spectrometer using a silicon detector in the wavelength range between 600 and 1250 nm and an MCT detector in the wavelength range between 1250 and 7000 nm. For the latter measurements an infrared Hyperion microscope was employed with numerical aperture NA = 0.4. This leads to an ill-defined incident wave-vector in contrast to the measurements performed with the ellipsometer where the incident wave-vector is well-defined within 0.01°. In Figure 2a and b the results of the reflectance measurements over the entire frequency range for the different square sizes a are shown together with the reflectance of the bare Si/SiO_2 substrate and that of a 20 nm thick closed gold film for comparison. The reflectance of the bare substrate is governed by interference effects in the 300 nm thick SiO_2 layer. The reflectance of the closed 20 nm thick Au film resembles that of a thick Au film with a flat reflectance of roughly 95% in the infrared and the characteristic interband transitions in the visible. Both curves can be satisfactorily modeled by a two- (Si/SiO_2) and three-layer ($Si/SiO_2/Au$) system with the above-mentioned thicknesses by the Woollam VASE software (Figure 2c and d). In

DOI: 10.1021/acsphotonics.6b00198
ACS Photonics 2016, 3, 1109–1115

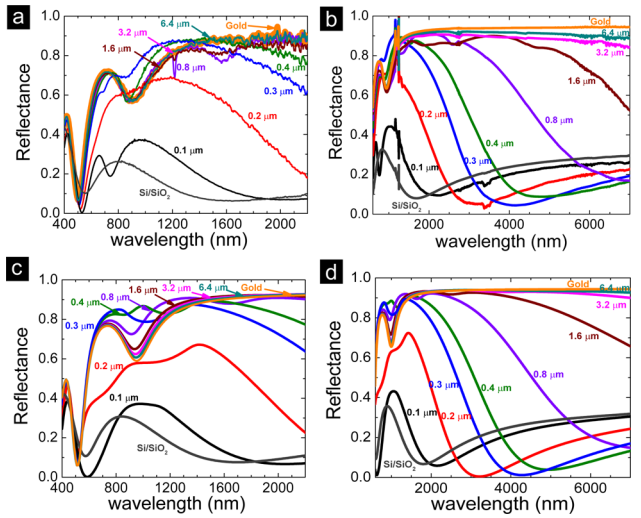

Figure 2. (a) Experimental and (c) simulated reflectance at an angle of incidence of 30° between 400 and 2200 nm for square patterns with different square size a, for the bare Si/SiO_2 substrate (dark gray) and for a 20 nm thick closed gold film (orange). (b) Experimental and (d) simulated reflectance at normal incidence between 600 and 7000 nm for square patterns with different square size a, for the bare Si/SiO_2 substrate (dark gray) and for a 20 nm thick closed gold film (orange).

Figure 2b the reflectance of the bare substrate shows a maximum around 835 nm, it goes through a minimum at about 1680 nm, and it rises again, reaching a plateau with an intensity of 0.3. Interestingly, the reflectance of the 0.1 μm square array shows a very similar trend to that of the bare substrate with a slightly larger, red-shifted reflectance maximum followed by a broad, lower reflectance minimum at about 2200 nm compared to that of the bare substrate. Combining transmittance and reflectance measurements reveals also that, in the wavelength region where the reflectance of the samples is lower than that of the bare substrate, the absorbance of the square arrays is higher than that of the bare substrate (see Supporting Information). The presence of the plasmonic resonance of the small squares is apparent to the blue side of the reflectance maximum. Although the gold filling factor of the 0.1 μm square pattern is already 70%, it behaves as a dielectric layer supporting a plasmonic resonance. The dielectric behavior corresponds to an increase of the effective thickness of the SiO_2 layer. With increasing square size a (gold filling factor f_m) the patterned films start to absorb more and more in the near-infrared, leading to an increased reflectance until nearly metallic behavior is reached. The reflectance of the two samples with the largest squares (a = 3.2 and 6.4 μm) is close to that of the 20 nm thick closed gold film especially in the visible and near-infrared range (Figure 2a). However, even though for a = 6.4 μm the filling factor reaches 99.5%, the reflectance at large wavelength decreases, in contrast to the expected behavior for a Drude metal; that is to say, the light does "sense" the presence of the gaps (Figure 2b). A real drop of the reflectance is observed for squares with a between 0.2 and 1.6 μm, with the intensity reaching the lowest value of 5% for a = 0.2 μm. Moreover, for all patterned films up to a = 0.8 μm the reflectance at the minimum is well below that of the bare substrate; that is, they act as an effective antireflection coating for the infrared light. The results discussed up to now can in principle be gained from the FTIR measurements alone shown in Figure 2b. The drawback of this measurement is that the reflectance is obtained under an IR microscope with NA = 0.4, and therefore the results are averaged over a large range of incident angles. Under these conditions specific features stemming from the periodicity of our patterned samples, namely, the influence of the Rayleigh–Wood's anomalies expected for grating structures, are smeared out.[10,11] In the limited frequency range of the ellipsometer the overall reflectance measured at an angle of incidence of 30° with p-polarized light shown in Figure 2a is almost the same as that of the reflectance of Figure 2b measured with the FTIR spectrometer, but for the same specimens extra features appear. In the samples with a = 0.8 and 1.6 μm for example, additionally sharp dips at about 1200 nm can clearly be identified in Figure 2a that are not present in the FTIR measurements. The dips can be attributed to the Rayleigh–Wood's anomalies. This can be clearly confirmed by additional dispersion measurements. In Figure 3c a reflectance contour

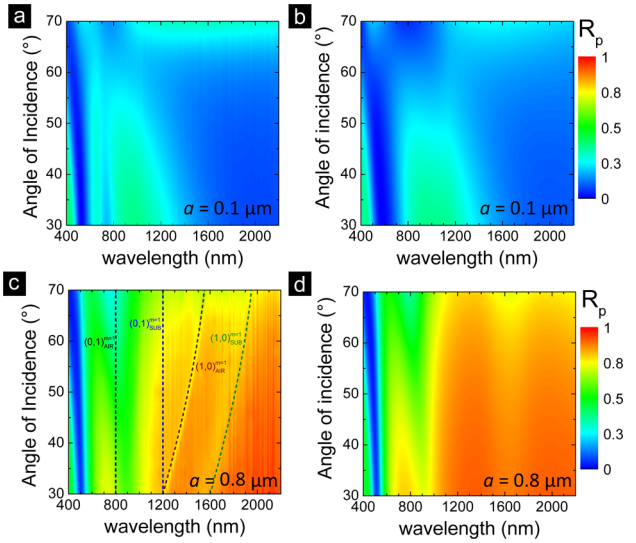

Figure 3. Contour plot of the (a) measured and (b) modeled reflectance with p-polarized light between 30° and 70° in steps of 2° in the spectral range between 400 and 2200 nm for the square array with size a = 0.1 μm. Contour plot of the (c) measured and (d) modeled reflectance with p-polarized light between 30° and 70° in steps of 2° in the spectral range between 400 and 2200 nm for the square array with size a = 0.8 μm. The dashed lines in (c) correspond to Rayleigh–Wood's anomalies.

plot of the 0.8 μm square array measured with p-polarized light over an angle of incidence between 30° and 70° in steps of 2° is displayed. The spectral positions of the Rayleigh–Wood's anomalies are additionally plotted in Figure 3c. A clear influence of the grating structure can be seen due to the effect of the first substrate modes and, in particular, of the air modes. The dispersion of the Rayleigh–Wood's anomalies is described by the equation $\lambda_R = p/m^*[n + \sin(\theta)]$, which determines the wavelength at which a diffracted order becomes tangent. Here p is the period of the grating (0.8 μm), m is the diffraction order, n is the refractive index (n_{SiO2} = 1.5 for the substrate and n = 1 for the air), and θ is the angle of incidence. For the smaller squares as well as for the larger squares the Rayleigh–Wood's anomalies lie outside the spectral range covered by the ellipsometer. From Figure 3, one can also see that the antireflective properties of all the samples hold over a broad range of angles of incidence. Similarly to the description given in Figure 2, the 0.1 μm sample reflectance contour plot is

DOI: 10.1021/acsphotonics.6b00198
ACS Photonics 2016, 3, 1109–1115

characterized by an interference pattern due to the SiO_2 layer, slightly modified by the presence of the gold squares. The main reflectance maximum is present up to 60° and follows the expected dispersion. The plasmonic resonance, due to the excitation of the localized surface plasmon resonance of the small gold squares, is nondispersive, as expected. The antireflective properties of the investigated sample hold over a broad range of wavelengths and cover a broad range of angles of incidence spanning from normal incidence to very large angle, for s-polarized light as well (see the Supporting Information). The larger squares are dominated by the red-shift of the reflectance minimum to wavelengths outside the measured range and are therefore characterized by an increased reflectance in the near-infrared range, independently of the angle of incidence (Figure 3c). The dispersive behavior of the other samples is very similar (not shown).

SIMULATION AND DISCUSSION

In order to retrieve a reliable model for the effective optical response of the samples, the ellipsometric data together with the reflectance data obtained by the ellipsometer as well as from the FTIR spectrometer were simultaneously fitted by a three-layer model composed of a 20 nm thick BEMA layer, a 300 nm SiO_2 layer, and the 1 mm Si substrate. In the BEMA, the complex effective dielectric functions ε_{eff} of the nanostructured Au films are calculated by

$$f_m \frac{\varepsilon_a - \varepsilon_{eff}}{\varepsilon_{eff} + L(\varepsilon_a - \varepsilon_{eff})} + (1 - f_m)\frac{\varepsilon_b - \varepsilon_{eff}}{\varepsilon_{eff} + L(\varepsilon_b - \varepsilon_{eff})} = 0 \quad (1)$$

where L is the depolarization factor, which relates the polarizability of the metallic inclusions (gold squares) in the direction of the applied field to their shape, f_m is the filling factor of the metallic squares, ε_a is the complex dielectric constant of the gaps (air, $\varepsilon_a = 1$), and ε_b is the complex dielectric function of a 20 nm closed gold film. The permittivity of the Au film has been obtained by modeling an unstructured part of the same sample. The only free fit parameters left in our BEMA model are L and f_m. Figure 4a and b show the results for

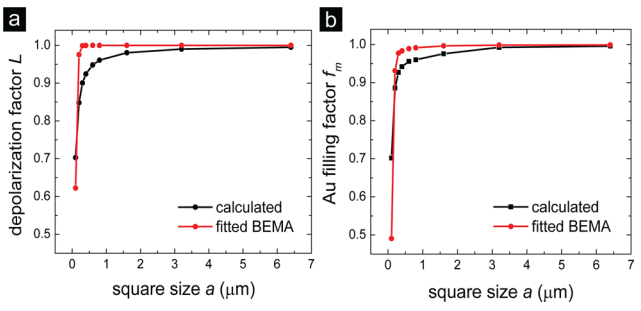

Figure 4. Comparison between (a) depolarization factor L and (b) gold filling factor f_m used in the model and the ones calculated using the geometrical parameters extracted from the SEM images for the different samples.

L and f_m obtained by fitting all investigated samples with respect to the square size. Both parameters rapidly increase to 1 with increasing a, reaching in both cases maximum value of 0.995. The interference effects responsible for the antireflective properties of the samples can be explained by the BEMA model as a result of the particular effective permittivity of the gold square arrays, which follows a similar trend to that of semicontinuous gold films below the percolation threshold.[7] The effective ε_1 increases with the square size a for longer wavelengths, whereas the ε_2 peak gets broader and larger while red-shifting (see the Supporting Information). The suppressed reflectance occurs in the frequency range where the gold square patterns act as a mere dielectric layer with positive ε_1 and very low ε_2. In the case of the square array with size $a = 0.1$ μm, almost no light is absorbed by the gold squares as a result of the combination of a positive ε_1 and a zero value of ε_2 over the whole infrared range. As a increases, the gold squares absorb more and more incoming light over a broader range of wavelengths, resulting in an increased reflectance up to values comparable to that of a closed gold film. However, the metallic behavior characterized by a negative ε_1 and a large absorption is never reached fully over the whole wavelength range, leading to a shift of the minimum of the reflectance toward higher wavelengths outside the displayed range (not shown). The simulated reflectance obtained with the BEMA model is plotted in Figure 2c and d. Although in the BEMA model there are only two free fit parameters, L and f_m, the calculated reflectance nearly perfectly coincides with the measured reflectance over the whole frequency range from 400 up to 7000 nm. In order to assign effective medium properties to our nanostructured Au films, the BEMA model has to work also over a broad range of angles of incidence. Figure 3b and d display the simulated p-polarized reflectance in the range between 400 and 2200 nm at an angle of incidence varying from 30° to 70° for the square arrays with $a = 0.1$ and 0.8 μm, respectively. The comparison reveals a very good quantitative agreement between the experimental and simulated data for the two samples even over the broad k-range, confirming that the assignment of effective optical parameters is justified in this case. These conclusions are also valid for the other square sizes (not shown). Only the sharp features coming from the Rayleigh–Wood's anomaly marked with dashed lines in Figure 3c and the presence of the plasmonic resonances for the smaller squares are not reproduced by the simple BEMA, as it does not account for periodicity. In fact one would expect that the main limitation of the BEMA model in describing the optical behavior of ordered nanostructures is that their period must be much smaller than the wavelength of the incident radiation. Under this condition, diffraction effects are not present and the nanostructure can be treated as a homogeneous material with effective optical properties.[12,13] Due to these limitations, many complex methods have been developed to model the optical properties of two-dimensional gratings, such as rigorous couple-wave analysis[14] and discrete dipolar approximation.[15] On the other hand, Kravets et al. have already reported how an effective medium approach provides a surprisingly good qualitative description of the transmittance and reflectance in the visible and near-infrared range of a nanostructured one-dimensional metallic grating with low filling factors f and a period comparable to the wavelength, taking into account polarization-dependent dipole interactions between the stripes via the depolarization factor.[16] However, in their work the nanorods were separated by more than 100 nm; hence the near-field coupling between the grating lines should be small. Consequently, the assumption of a homogeneous background field in which the particles are embedded still stands and an effective medium theory can, in principle, be applied. As further proof of the correctness of our isotropic BEMA model, azimuthal-dependent reflectance measurements were performed for the samples with $a = 0.1$ and 0.8 μm (see the

DOI: 10.1021/acsphotonics.6b00198
ACS Photonics 2016, 3, 1109–1115

Supporting Information). Although our samples are two-dimensional periodic arrays, the optical response of the samples is totally isotropic, except for the azimuth-dependent effect of the Rayleigh-Wood's anomalies on the reflectance of the sample with $a = 0.8$ μm. The result confirms the choice of an isotropic BEMA model for the analyses of the optical properties of the structures.

The depolarization factor L and the filling factor f_m were treated as pure fitting parameters up to now; on the other hand, they both have a physical meaning, and they can, in principle, be calculated from the geometry of the sample. In our effective medium model the gold squares can be approximated by very flat disks of dimensions a along the x- and y-directions and $t \ll a$ along the z-direction. In general, effective medium theories assume that the fluctuations of the local field around its mean value should average to zero and that the inclusions are relatively far away from each other so that interactions are simply not present. Under this assumption the geometrical depolarization factor L of a flat isolated inclusion (oblate spheroid) oriented perpendicular to the applied field can be deduced from its three axes according to the formula

$$L = \frac{1 + r^2}{r^2}\left(1 - \frac{1}{r}\tan^{-1} r\right) \quad (2)$$

where $r^2 = (x^2/z^2) - 1$.[17] In general, $L \to 1$ in the case of flat oblate spheroids oriented perpendicular to the applied field, whereas $L \to 0$ for an electric field parallel to its plane. The effective depolarization factor L calculated with eq 2 and the gold filling factor f_m for the different samples calculated from the geometrical parameters of the square arrays extracted from the SEM images of the samples are plotted in Figure 4 together with the corresponding values of the fitted parameters obtained by fitting the BEMA model to the measured optical data. A metallic inclusion in an electric field will produce a screening charge at its boundaries in opposition to the applied electric field. If all the boundaries between the inclusions and the matrix are parallel to the applied field, little screening charge is developed; on the contrary, if all the boundaries are perpendicular to the applied field, the screening effect will be maximum and the electric field will not see the inclusions.[18] These two limits of "no screening" and "maximum screening", respectively, are defined by the Wiener bounds describing the effective permittivity of a two-phase composite regardless of composition and microstructure.[18] In our samples composed of subwavelength two-dimensional square arrays, a propagating light beam with electric field polarized parallel to the surface of the squares will always have the polarization perpendicular to the boundary; hence $L \to 1$ in all directions. This leads to a new effective depolarization factor L_{eff}, which still can be deduced from eq 2 by considering the squares as oblate spheroids with the calculated depolarization factor L always associated with the axis of rotation that is parallel to the applied field ($L_{eff} = L$).[19] The agreement between the values calculated from pure geometry and the ones obtained by fitting the experimental data is very good. The same goes for the geometrical f_m and the effective f_m obtained from the BEMA model. The main difference is that the fitted effective values for L and f_m increase even faster to 1 with increasing square size than the geometrical estimated. In the BEMA theory the critical filling factor f_c defining the percolation threshold and the depolarization parameter L describing the shape of the inclusions are closely connected by $L = f_c$ (2). In the limit of an infinite flat disk ($a \to \infty$), e.g., corresponding to a closed metallic film, both parameters should therefore become 1. In our artificial nanostructured Au films the percolation is prevented by deliberate cuts, and therefore this condition is never fulfilled. The suppression of the percolation via the presence of the roughly 20 nm wide gaps prevents the development of so-called "hot spots", i.e., areas with very small gaps leading to huge field enhancement, accompanying the transition into the metallic state, as it is normally observed in the case of random percolating two-dimensional nanocomposites.[20] In other words, although some limited field enhancement inside the gaps is expected and the condition of a homogeneous mean field surrounding the gold squares should in principle not be valid anymore, the gaps are too large to create hot spots.[21] Due to the homogeneous gap width, all the squares are indeed embedded in a homogeneous background field, and therefore the BEMA model still holds.

As it was already shown by Efros et al. in their seminal paper, the real part of the permittivity is expected to diverge at the percolation threshold.[22] The divergence can be qualitatively interpreted by the increased capacitive coupling between adjacent particles with increasing filling factor. Each pair of nearest particles forms a capacitor, with an effective surface that tends to infinity and its distance to zero at the percolation threshold. Hence, for random samples, the effective capacity of the system diverges. In our artificial system, the effective surface as well as the distance between the squares is controlled by the geometry of the nanostructure, and one needs to be careful with the interpretation framework of the simple capacitor picture. Since the percolation threshold is pushed toward 1, the effective real part of the permittivity keeps on increasing with the filling factor, i.e., with the square size. In Figure 5, the divergence of the real part of the dielectric function ε_1 obtained at $\lambda = 7$ μm is shown as a function of f_m. In principle, the trend is the same as in the case of randomly evaporated Au films except that with an artificially suppressed percolation much higher maximum values of the permittivity can be reached.[7] The highest value of ε_1 we obtained for the 6.4 μm square is 1420, which is 1 order of magnitude larger than in random metal−dielectric nanostructures and is, to the best of our knowledge, the highest value ever measured for a metallodielectric composite at infrared frequencies.

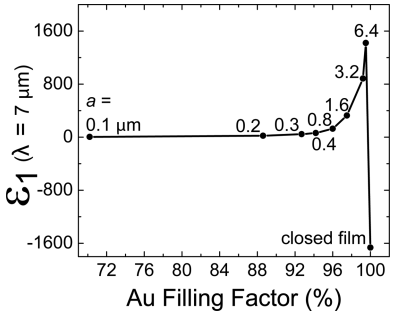

Figure 5. Divergence of the real part of the dielectric function ε_1 obtained at $\lambda = 7$ μm as a function of the calculated gold filling factor for the different square arrays of size a. The ε_1 for a closed gold film of 20 nm thickness is also shown.

CONCLUSION

In summary, we have shown that a 2D periodic mesh of 20 nm wide gaps in a 20 nm thick Au film interrupting the dc

DOI: 10.1021/acsphotonics.6b00198
ACS Photonics 2016, 3, 1109−1115

conductivity dramatically changes the optical response in the visible and infrared frequency range. Preventing percolation, tunable antireflective properties can be achieved for a broad range of angles of incidence and over a wide frequency range in the infrared. The entire optical behavior can be modeled over the whole frequency range and a large variety of angles of incidence, by an effective optical permittivity using a simple isotropic BEMA approach with only two adjustable parameters, namely, the filling factor f_m and the effective depolarization factor L, which takes into account the strong interaction between the gold squares. The suppressed percolation leads to the divergence of the real part of the dielectric function ε_1 in the infrared frequency range, reaching values 1 order of magnitude higher than that obtained in random metal−dielectric nanostructures.

METHODS

The square arrays were fabricated using a Jeol JBX6300FS electron beam lithography system on a doped silicon substrate with a thermally grown 300 nm thick silicon dioxide top layer. Two different resists were applied on the substrate in two consecutive steps via spin-coating. First 80 nm of poly(methyl methacrylate) (PMMA) 950k was spin coated on the substrate followed by a layer of 30 nm of HSQ. In order to prevent resist intermixing, the layer of PMMA was prebaked on a hot plate at 160 °C for 4 min before the layer of HSQ was spin-coated. The square arrays were then exposed into the resist over a total exposed area of 2.5 mm by 1.5 mm for the samples with a square size of approximately 0.1 and 0.2 μm. All the other samples were exposed over a total area of 1.5 mm by 1.5 mm. A large patterned area is crucial to perform optical measurements with the ellipsometer, in particular at high angles of incidence. The exposure parameters were 100 kV of acceleration voltage and a dose of 8 mC/cm^2. The exposure is followed by the development of the HSQ top layer in Microposit MF322, which results in a fishnet-like grid. To stop the development, the sample is rinsed in an overflow bath with deionized water for 30 s. Using any organic solvent for rinsing would dissolve the PMMA immediately, as the PMMA is strongly overexposed. In order to transfer the HSQ mask into the PMMA, reactive ion etching is applied. Thermal evaporation was then used to deposit a 2 nm thick adhesion layer of Cr with an evaporation rate of 1 Å/s and 20 nm of Au with an evaporation rate of 2 Å/s. Finally, a 1 h long *N*-ethyl-2-pyrrolidone bath at 80 °C was used during the lift-off, followed by low-power ultrasonic agitation for a few seconds at the end of the process. The sample was rinsed in acetone and 2-propanol and dried with a N_2 spray gun.

ASSOCIATED CONTENT

Supporting Information

The Supporting Information is available free of charge on the ACS Publications website at DOI: 10.1021/acsphotonics.6b00198.

Effective dielectric constants extracted from the BEMA model; comparison of the measured and simulated reflectance with s-polarized light for the sample with a = 0.1 μm; azimuthal angle dependent reflectance measured with p-polarized light at an angle of incidence of 30° for the samples with a = 0.1 μm and a = 0.8 μm; absorbance between 1500 and 7000 nm (PDF)

AUTHOR INFORMATION

Corresponding Author

*E-mail: gompf@pi1.physik.uni-stuttgart.de.

Present Address

§Chalmers University of Technology, MC2 Kemivägen 9, 41285 Gothenburg, Sweden.

Notes

The authors declare no competing financial interest.

ACKNOWLEDGMENTS

We acknowledge financial support by the Deutsche Forschungsgemeinschaft via DFG DR228/38-1. A.B. acknowledges the Carl Zeiss Foundation for support.

REFERENCES

(1) Brosseau, C. Modelling and simulation of dielectric heterostructures: a physical survey from an historical prospective. *J. Phys. D: Appl. Phys.* **2006**, *39*, 1277−1294.

(2) Choy, T. C. *Effective Medium Theory: Principles and Applications*; Oxford University Press, 1999.

(3) Clerc, J. P.; Giraud, G.; Laugier, J. M.; Luck, J. M. The electrical conductivity of binary disordered systems, percolation clusters, fractals and related models. *Adv. Phys.* **1990**, *39*, 191−309.

(4) De Zuani, S.; Peterseim, T.; Berrier, A.; Gompf, B.; Dressel, M. Second harmonic generation enhancement at the percolation threshold. *Appl. Phys. Lett.* **2014**, *104*, 241109.

(5) Scher, H.; Zallen, R. Critical density in percolation process. *J. Chem. Phys.* **1970**, *53*, 3759−3761.

(6) Gompf, B.; Beister, J.; Brandt, T.; Pflaum, J.; Dressel, M. Nanometer-thick Au-films as antireflection coating for infrared light. *Opt. Lett.* **2007**, *32*, 1578−1580.

(7) Hövel, M.; Gompf, B.; Dressel, M. Dielectric properties of ultrathin metal films around the percolation threshold. *Phys. Rev. B: Condens. Matter Mater. Phys.* **2010**, *81*, 035402.

(8) De Zuani, S.; Reindl, T.; Rommel, M.; Gompf, B.; Berrier, A.; Dressel, M. High-Order Hilbert Curves: Fractal Structures with Isotropic, Tailorable Optical Properties. *ACS Photonics* **2015**, *2*, 1719−1724.

(9) Rommel, M.; Nilsson, B.; Jedrasik, P.; Bonanni, V.; Dmitriev, A.; Weis, J. Sub-10 nm resolution after lift-off using HSQ/PMMA double layer resist. *Microelectron. Eng.* **2013**, *110*, 123−125.

(10) Wood, R. W. On a remarkable case of uneven distribution of light in diffraction grating spectrum. *Philos. Mag.* **1902**, *4*, 396−402.

(11) Rayleigh, L. On the dynamical theory of gratings. *Proc. R. Soc. London, Ser. A* **1907**, *79*, 399−416.

(12) Grann, E. B.; Moharam, M. G.; Pommet, D. A. Optimal design for antireflective tapered two-dimensional subwavelength grating structures. *J. Opt. Soc. Am. A* **1995**, *12*, 33310.1364/JOSAA.12.000333.

(13) Lalanne, P.; Lemercier-lalanne, D. On the effective medium theory of subwavelength periodic structures. *J. Mod. Opt.* **1996**, *43*, 2063−2085.

(14) Li, L. Use of Fourier series in the analysis of discountinuous periodic structures. *J. Opt. Soc. Am. A* **1996**, *13*, 1870−1876.

(15) Gomez-Medina, R. Extraordinary optical reflection from sub-wavelength cylinder arrays. *Opt. Express* **2006**, *14*, 3730.

(16) Kravets, V. G.; Schedin, F.; Grigorenko, A. N. Plasmonic blackbody: almost complete absorption of light in nanostructured metallic coatings. *Phys. Rev. B: Condens. Matter Mater. Phys.* **2008**, *78*, 205405.

(17) van de Hulst, H. C. *Light Scattering by Small Particles*; Dover Publications, Inc., 1981.

(18) Aspnes, D. E. Local-field effects and effective-medium theory: a microscopic perspective. *Am. J. Phys.* **1982**, *50*, 704−709.

(19) Cohen, R. W.; Cody, G. D.; Coutts, M. D.; Abeles, B. Optical properties of granular silver and gold films. *Phys. Rev. B* **1973**, *8*, 3689−3701.

DOI: 10.1021/acsphotonics.6b00198
ACS Photonics 2016, 3, 1109−1115

(20) Shalaev, V. M. *Optical Properties of Nanostructures Random Media*; Springer, 2002.
(21) Romero, I.; Aizpurua, J.; Bryant, G. W.; Garcia de Abajo, F. J. Plasmons in nearly touching metallic nanoparticles: singular response in the limit of touching dimers. *Opt. Express* **2006**, *14*, 9988−9999.
(22) Efros, A.; Shklovskii, B. Critical behaviour of conductivity and dielectric constant near the metal-non-metal transition threshold. *Phys. Status Solidi B* **1976**, *76*, 475−485.

DOI: 10.1021/acsphotonics.6b00198
ACS Photonics 2016, 3, 1109−1115